EJNMMI Research

ORIGINAL RESEARCH Open Access

Bone marrow cell homing to sites of acute tibial fracture: ^{89}Zr-oxine cell labeling with positron emission tomographic imaging in a mouse model

Kingsley O. Asiedu[1], Munira Ferdousi[1], Phuongnga T. Ton[1], Stephen S. Adler[2], Peter L. Choyke[1] and Noriko Sato[1*]

Abstract

Background: Bone fracture healing is dependent upon the rapid migration and engraftment of bone marrow (BM) progenitor and stem cells to the site of injury. Stromal cell-derived factor-1 plays a crucial role in recruiting BM cells expressing its receptor CXCR4. Recently, a CXCR4 antagonist, plerixafor, has been used to mobilize BM cells into the blood in efforts to enhance cell migration to sites of injury presumably improving healing. In this study, we employed zirconium-89 (^{89}Zr)-oxine-labeled BM cells imaged with positron emission tomography (PET)/computed tomography (CT) to visualize and quantitate BM cell trafficking following acute bone injury and to investigate the effect of plerixafor on BM cell homing. Unilateral 1-mm incisions were created in the distal tibia of mice either on the same day (d0) or 24 h (d1) after ^{89}Zr-oxine-labeled BM cell transfer ($n = 4–6$, $2–2.3 \times 10^7$ cells at 9.65–15.7 kBq/10^6 cells). Serial microPET/CT imaging was performed and migration of ^{89}Zr-labeled cells to the bone injury was quantified. The effects of three daily doses of plerixafor on cell trafficking were evaluated beginning on the day of fracture generation ($n = 4–6$). The labeled cells localizing to the fracture were analyzed by flow cytometry and immunohistochemistry.

Results: In d0- and d1-fracture groups, 0.7% and 1.7% of administered BM cells accumulated within the fracture, respectively. Plerixafor treatment reduced BM cell migration to the fracture by approximately one-third ($p < 0.05$ for both fracture groups). Flow cytometry analysis of donor cells collected from the injured site revealed a predominance of CD45$^+$ stem/progenitor cell populations and subsequent histological analysis demonstrated the presence of donor cells engrafted within sites of fracture repair.

Conclusion: ^{89}Zr-oxine labeling enabled visualization and quantitation of BM cell recruitment to acute fractures and further demonstrated that plerixafor plays an inhibitory role in this recruitment.

Keywords: Zirconium-89 (^{89}Zr)-oxine, Bone injury, Bone marrow cell, Cell tracking, Positron emission tomography, Zirconium-89, Fracture

Background

Bone healing is a multistep physiological process that begins immediately following injury. Bone fracture triggers an immunological cascade beginning with signaling by pro-inflammatory cytokines such as interleukin 1 (IL-1), IL-6, and tumor necrosis factor-α (TNF-α), secreted by macrophages and periosteal cells [1–3], which, in turn, recruit inflammatory and fibrogenic cells to the injury site [4]. Bone remodeling and healing are preceded by angiogenesis, chondrogenesis, and osteogenesis. These processes are contingent on the migration and proliferation of hematopoietic stem cells (HSCs), endothelial progenitor cells (EPCs), and periosteum-derived mesenchymal stem cells (MSCs) from the bone marrow (BM) or circulation [5]. The blood vessel walls and nearby soft-tissues also act as sources of MSCs [6–8]. For the migration of HSC, MSC, and EPC and subsequent homing to the fracture region, stromal

* Correspondence: saton@mail.nih.gov
[1]Molecular Imaging Program, Center for Cancer Research, National Cancer Institute, National Institutes of Health, NIH, Building 10, Room B3B406, Bethesda, MD 20892-1002, USA
Full list of author information is available at the end of the article

cell-derived factor-1 (SDF-1) has been reported to play a crucial role. The interaction of SDF-1 in the injured stroma with CXCR4 expressed on these stem cells results in the accumulation of these cells at the fracture site [5, 9, 10].

Investigators have examined blockade of CXCR4 to mobilize stem and progenitor cells to enhance their recruitment to the fracture and to promote fracture healing. Some studies report that increasing the number of mobilized stem and progenitor cells facilitates the repair process [11–13]. Others, however, report opposite results [14, 15]. For example, mice treated with either SDF-1 neutralizing antibody or TF14016, a CXCR4 antagonist, demonstrated decreased stem cell engraftment and bone formation [15]. These data suggest that CXCR4 inhibition and subsequent mobilization of $CXCR4^+$ cells may, or may not, improve bone injury healing by releasing high number of stem/progenitor cells into the circulation, thus making more available for localization within the injury site. To address this question, radiolabeled cells can be used to track and quantify recruitment of stem/progenitor cells to the bone injury with and without CXCR4 blockade. We have previously reported a method of cell labeling using ^{89}Zr-oxine followed by positron emission tomography (PET) that can label various cell types without altering their cellular viability or function [16]. Using this technology, we have successfully visualized BM cell migration in murine models of BM transplantation [17]. Additionally, it was demonstrated that a CXCR4 inhibitor, plerixafor, mobilized these 89 Zr-oxine-labeled BM cells into the circulation [17]. To explore the migration of BM cells to sites of bone injury, we employed ^{89}Zr-oxine cell labeling of BM cells and PET imaging in bone injury model. This method enabled the quantification of the number of cells migrating to the fracture site. We employed two tibial injury/BM cell transfer experimental schemes; in one model, mice received a radiolabeled BM cell transfer followed 1 day later by incisional injury of the tibia. In the second model, BM cell transfer was performed immediately after the tibial injury. Using these two schemes, we examined the trafficking of BM cells and the effect of plerixafor on the short-term BM cell homing to the bone injury.

Methods

Mice

C57BL/6 wild type and green fluorescence protein (GFP) transgenic mice were purchased from Jackson Laboratories (Bar Harbor, ME).

Fracture generation

All procedures were approved by the institutional animal care and use committee and were compliant with the humane use of animals. A fracture of the tibia was created as previously described [18] with minor modifications. In brief, the mice were anesthetized with isoflurane inhalation and the left hind limb surface was soaked with 10% Povidone-iodine solution (Purdue Pharma L.P., Stamford, CT). Using a surgical scalpel (WESTNET, Inc., Canton, MA), an approximately 1-mm-long incision was created in the medial side of the left distal tibia without cutting entirely through the bone. In some mice, the incision was made in the soft-tissue without reaching the tibia. Mice remained mobile after the surgery.

^{89}Zr-oxine synthesis

$^{89}ZrCl_4$ was produced at the institutional cyclotron facility. ^{89}Zr-oxine complex was synthesized from oxine and $^{89}ZrCl_4$ as previously described [16]. Briefly, 4 μl of 20% tween 80 solution (Sigma-Aldrich, St. Louis, MO) and 102 μl of 20 mM oxine in 0.04 N HCl were mixed in a tube, and then 60 ul of $^{89}ZrCl_4$ (37–74 kBq) was added and vortexed. The resulting solution was neutralized to pH 7.0–7.5 by adding 500 mM $NaHCO_3$ in portions with incremental vortexing.

BM cell labeling with ^{89}Zr-oxine

BM cells were flushed from femurs and tibias of donor mice. Red blood cells were lysed using ammonium-chloride-potassium (ACK) lysis solution (Thermo Fisher Scientific Inc., Waltham, MA) and the BM cells were washed in phosphate-buffered saline (PBS). Cell labeling with ^{89}Zr-oxine complex was performed to achieve the labeling doses optimized for the BM cells in the previous study [17]. Cells were incubated with ^{89}Zr-oxine complex at 45 kBq/10^6 cells in PBS at 30:1 cell suspension-to-^{89}Zr-oxine solution volume ratios for 20 min at room temperature. Labeled cells were washed twice in RPMI culture media (Life Technologies, Grand Island, NY) supplemented with 10% fetal calf serum (Gemini Bio Products, Sacramento, CA), 100 IU/mL penicillin, 100 μg/mL streptomycin (Life Technologies), and 50 μM 2-mercaptoethanol (Sigma-Aldrich, St. Louis, MO). ^{89}Zr-oxine-labeled BM cells were transferred to mice intravenously ($2–2.3 \times 10^7$ cells at 9.65–15.7 kBq/10^6 cells). BM cells collected from wild type were used unless specified that GFP transgenic mice were used as donors.

MicroPET/CT imaging of transferred ^{89} Zr-oxine-labeled BM cells

One group of mice received ^{89}Zr-oxine-labeled BM cell administration followed 1 day later by tibial injury (d1-fracture group). MicroPET/CT imaging (BioPET, Bioscan, Washington, DC) was performed 1 day after the cell transfer, before and after the injury, and on days 2 and 5. Another group of mice received ^{89}Zr-oxine-labeled BM

cells immediately after the tibial injury (d0-fracture group) followed by microPET/CT imaging on days 0, 1, 2, and 5. A 5-min emission PET scan per bed position was performed for a total of two bed positions on day 0, using a 400–700 keV energy window. On days 1, 2, and 5, scan time per bed position was increased to 6, 7.5, and 12.5 min, respectively, to account for radioactive decay. The acquired images were reconstructed using a three-dimensional ordered-subsets expectation maximization algorithm. VivoQuant software (inviCRO LLC, Boston, MA) was used to fuse the maximum intensity projection PET images with CT images.

Quantitation of ^{89}Zr-oxine-labeled BM cell migration on microPET/CT images

Volumes of interest were drawn on the acquired images using VivoQuant and MIMvista (MIM software, Cleveland, OH) software. The percentage of injected cells migrated to the injury and organs were obtained from the quantitated radioactivity in the tissue corrected for decay divided by the injected dose. For the tibial fracture, corresponding contralateral tibia was used as a control. Signal-to-background ratios of the fracture or the contralateral control were calculated from maximum standardized uptake value (SUV) of the fracture or contralateral control against mean SUV of the muscle. For the bone marrow uptake, the skull, forelimbs distal to the shoulder joint, and fracture site were excluded from the quantitation.

Mobilization of BM cells by plerixafor

D1-fracture mice received an intravenous injection of 5 mg/kg of plerixafor (Adooq Bioscience, Irvine, CA) at days 1–3 after the BM cell transfer (d1-fracture-plerixafor group). For d0-fracture mice, plerixafor was injected on day 0 at the time of BM cell transfer, and on days 1 and 2 for a total of 3 doses (d0-fracture-plerixafor group).

Flow cytometry analysis of BM cells migrated to the fracture sites and spleen

Thirty-three million BM cells collected from GFP transgenic mice were transferred to wild-type hosts, in the d1- and d0-fracture models. Two days after cell transfer, BM cells were flushed and collected from the fractured section of tibia and the corresponding section of the contralateral non-fractured tibia. A 70 μm filter was used to create a single cell suspension. The femur of the contralateral side was also isolated and BM cells were collected. Spleen was harvested, homogenized, and passed through a 70 μm filter; red cells were lysed using ACK lysis solution. Collected cells were stained with antibodies against CD45, CD29, CD105, CD11b, Ly6C, and Ly6G or with lineage markers (CD3, NK1.1, Ly6G, CD2, CD5, B220). All antibodies were purchased from eBioscience (San Diego, CA). Data collected by a flow cytometer (FACSCalibur, Becton Dickinson, San Jose, CA) was analyzed using FlowJo software (Tree Star, Inc., Ashland, OR).

Histological analysis

^{89}Zr-oxine-labeled GFP^{+} BM cells were transferred to wild-type recipient mice and fracture was generated 1 day later. Tibias were removed from both fracture and non-fractured contralateral control sites at 1.5 and 7 weeks after the cell transfer and placed in 4% paraformaldehyde in PBS. Tibias were then embedded in paraffin and sectioned into 5-μm-thick slices. Following deparaffinization and rehydration, the slides were stained with hematoxylin and eosin (H&E). Immunohistochemistry staining was performed with an anti-GFP antibody conjugated with horseradish peroxidase (Life Technologies) followed by 3,3′-diaminobenzidine staining (GFP-IHC). Tibias from non-fractured wild-type and GFP transgenic mice were processed as controls.

Statistical analysis

Two-way repeated measure analysis of variance (ANOVA) with Sidak's multiple comparisons test was used to analyze the difference in BM cell accumulation at the fracture site compared to non-fractured tibia. Mann-Whitney test was used for comparing the peak BM cell accumulation values at the fracture with and without mobilization, and for analyzing the flow cytometry results between fractured- and non-fractured-tibias. P value, with adjustment for multiple comparison when comparing more than two groups, less than 0.05 was considered significant.

Results

BM cells labeled with ^{89}Zr-oxine show rapid homing to bone marrow and bone injury site

We first tracked ^{89}Zr-oxine-labeled BM cells transferred to mice without a fracture, as a control, by microPET/CT imaging beginning 1 day after the cell transfer ($n = 4$). In normal mice, ^{89}Zr-labeled BM cells were observed in the BM, spleen, and liver (Fig. 1a). When a group of mice underwent bone incision 1 day after the labeled BM cell transfer (d1-fracture group, $n = 4$), microPET/CT imaging showed redistribution of ^{89}Zr-labeled BM cells; the cells accumulated at the injury site within 24 h of the injury (2 days after cell transfer). The cells remained at the site until the end of the 5-day scanning period (Fig. 1b). To ascertain how the bone fracture affected the trafficking of circulating BM cells, a fracture was introduced and BM cells were immediately transferred (d0-fracture, $n = 4$). The BM cells homed to the BM, spleen, and liver, as well as to the fracture site starting 1 day after the

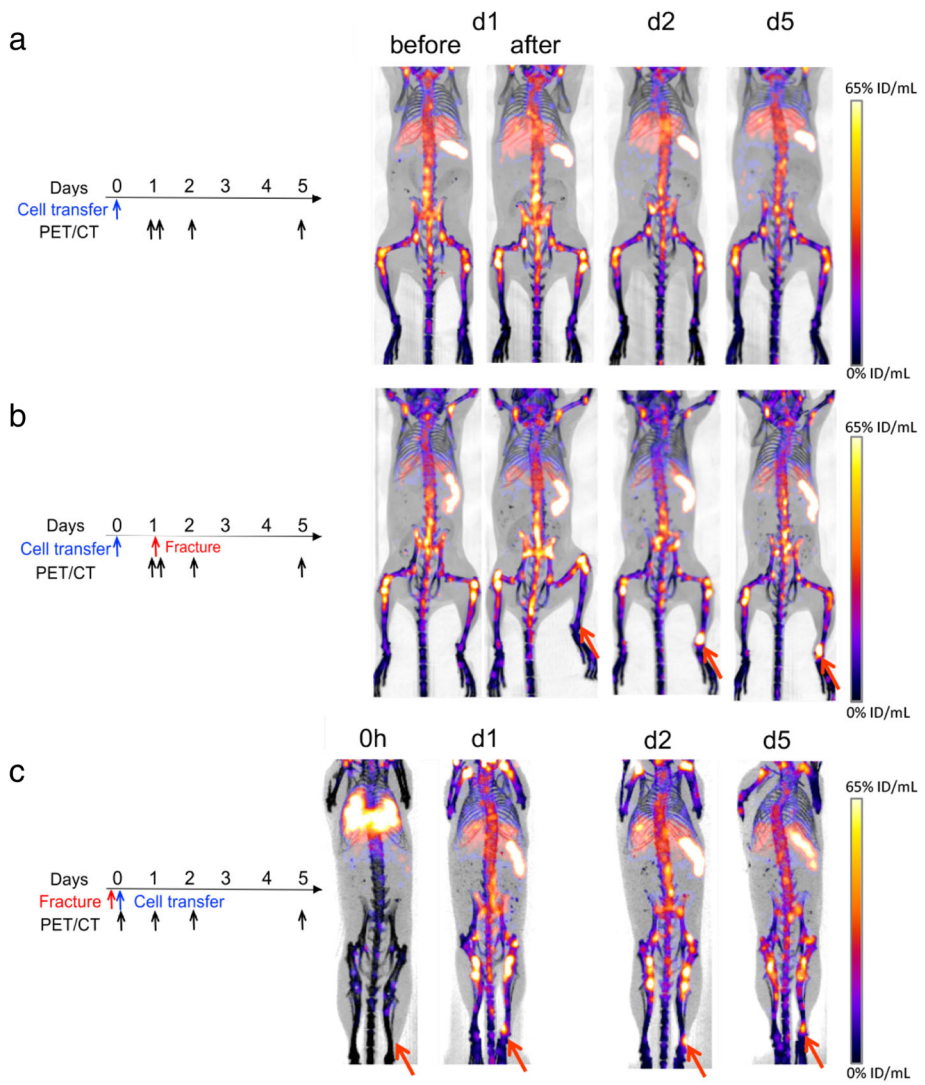

Fig. 1 BM cells labeled with ^{89}Zr-oxine rapidly accumulate at the bone fracture. **a** The regimen of BM cell transfer and microPET/CT imaging in control mice and acquired images is shown. The ^{89}Zr-oxine-labeled BM cells ($2–2.3 \times 10^7$ cells at 9.65–15.7 kBq/10^6 cells) administered intravenously homed to the BM, spleen, and liver by day 1 and remained in these organs until day 5 ($n = 4$). **b** The day 1-tibial fracture scheme and acquired microPET/CT images are shown. The ^{89}Zr-oxine-labeled BM cells distributed to the BM, spleen, and liver by day 1 as in the control mice. Following the tibial injury, labeled cells migrated to the fracture with peak accumulation by day 2, extending through day 5 ($n = 4$). **c** The day 0-tibial fracture scheme and acquired microPET/CT images are shown. The ^{89}Zr-oxine-labeled BM cells transferred immediately after the fracture generation trafficked to the injury site and remained at the site until day 5 ($n = 4$)

fracture/cell transfer (Fig. 1c). Again, the BM cells remained at the injury at least until the end of the 5-day imaging period. Quantitation of the radioactivity at the fracture site (Fig. 2a) revealed that approximately $1.7 \pm 0.5\%$ and $0.7 \pm 0.04\%$ of the injected labeled cells had migrated into the bone injury on day 2 for d1- and d0-fracture groups, respectively (Fig. 2b, c). ^{89}Zr-oxine-labeled cell accumulation at the injury was significantly higher than that at the non-fractured contralateral tibia in both groups ($p < 0.0001$ and $p < 0.001$ on days 2 and 5, respectively, in d1-fracture group; $p < 0.0001$ on days 1, 2, and 5 in d0-fracture group). Due to the very low background signals in the recipients, bone injury-to-background SUV ratios reached as high as 345 ± 114 and 250 ± 86 on day 2 in the d1- and d0-fracture groups (Additional file 1: Figure S1a, b). Cell distribution in the bone marrow, liver, and spleen remained fairly plateaued during the 5-day imaging period (Additional file 1: Figure S1c, d).

Mobilization of BM cells reduces cell migration to the fracture

To explore whether the SDF-1-CXCR4 system plays an important role in fracture healing by helping to mobilize

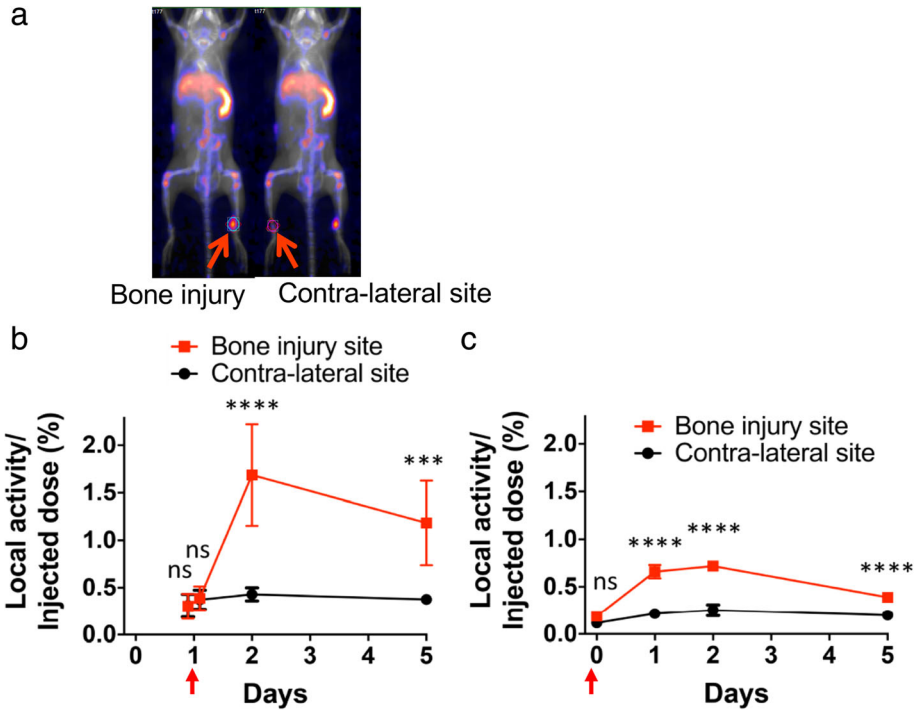

Fig. 2 Quantitation of microPET imaging reveals BM trafficking kinetics to the bone injury site. The percentage of ^{89}Zr activity accumulated at the fracture site was quantified by setting a volume of interest on the acquired PET/CT images (**a**) and correcting for radioactive decay. As an internal control, ^{89}Zr activity in the contralateral tibia was quantified. The BM cells highly accumulated at the fracture 1 day after the fracture generation in both the day 1-fracture (**b**) and day 0-fracture (**c**) schemes and gradually decreased thereafter. The BM cells preferentially accumulated at the fracture site compared to the contralateral control in both fracture models 1 day after the fracture generation ($n = 4$ in each group, $^{****}p < 0.0001$ and $^{***}p < 0.001$ with two-way repeated measure analysis of variance (ANOVA) with Sidak's multiple comparisons test. The arrows indicate the timing of bone injury generation)

BM cells from their niche into the peripheral blood, we investigated the effect of plerixafor on the accumulation of labeled cells at the injury site. In the d1-fracture-plerixafor group, microPET/CT images indicated accumulation of ^{89}Zr-oxine labeled-BM cells at the bone injury site under plerixafor injections (Fig. 3a, $n = 4$). By contrast, plerixafor administration reduced the accumulation of the circulating BM cells to the bone injury (d0-fracture-plerixafor groups, $n = 4$) and a very low ^{89}Zr signal was observed at the site (Fig. 3b). Quantitation of the images indicated that ^{89}Zr-labeled BM cells accumulated at the injury significantly more than the contralateral tibia in the d1-fracture-plerixafor group (Fig. 3c, $p < 0.001$ on day 2, $p < 0.01$ on day 5), but in d0-fracture-plerixafor group, BM cells accumulation at the injury was only slightly higher than the contralateral side (Fig. 3d. $p < 0.05$ on days 1 and 2). Plerixafor administrations significantly reduced the peak BM cell accumulation at the injury by 40% and 33% in d1- and d0-fracure-plerixafor groups, respectively: the peak was observed on day 2 in d1-fracture-plerixafor group (Fig. 3e, $p < 0.05$, $n = 6$) and on day 1 or day 2 in d0-fracture-plerixafor group (Fig. 3f, $p < 0.05$, $n = 6$).

Soft tissue injury alone does not induce BM cell accumulation at the fracture site

We then evaluated the effect of a soft tissue injury alone on the distribution of BM cells. ^{89}Zr-oxine-labeled BM cells were transferred to the mice immediately after injury ($n = 4$). As shown in Fig. 4, the labeled BM cells did not accumulate in the soft tissue injury site. This suggests that injuries to the bone are required to induce BM cell migration to the injured site.

Transferred BM cells with hematopoietic cell markers are detected at the site of fracture

Both hematopoietic and mesenchymal cell types are reported to be involved in fracture healing [15, 19, 20]. Therefore, we examined which subset of BM cells had localized to the fracture using GFP$^+$ donor cells in both d1- and d0-fracture groups ($n = 4$). Almost all of the GFP$^+$ BM cells detected at the fractured area, as well as contralateral control tibia, femur, and spleen, were hematopoietic (CD45$^+$) cells (Fig. 5a), containing undifferentiated (lineage marker negative: Lin$^-$) cells (Fig. 5b). Neither the CD45$^+$ cell fraction nor the Lin$^-$ cell fraction showed statistical differences between fractured- vs

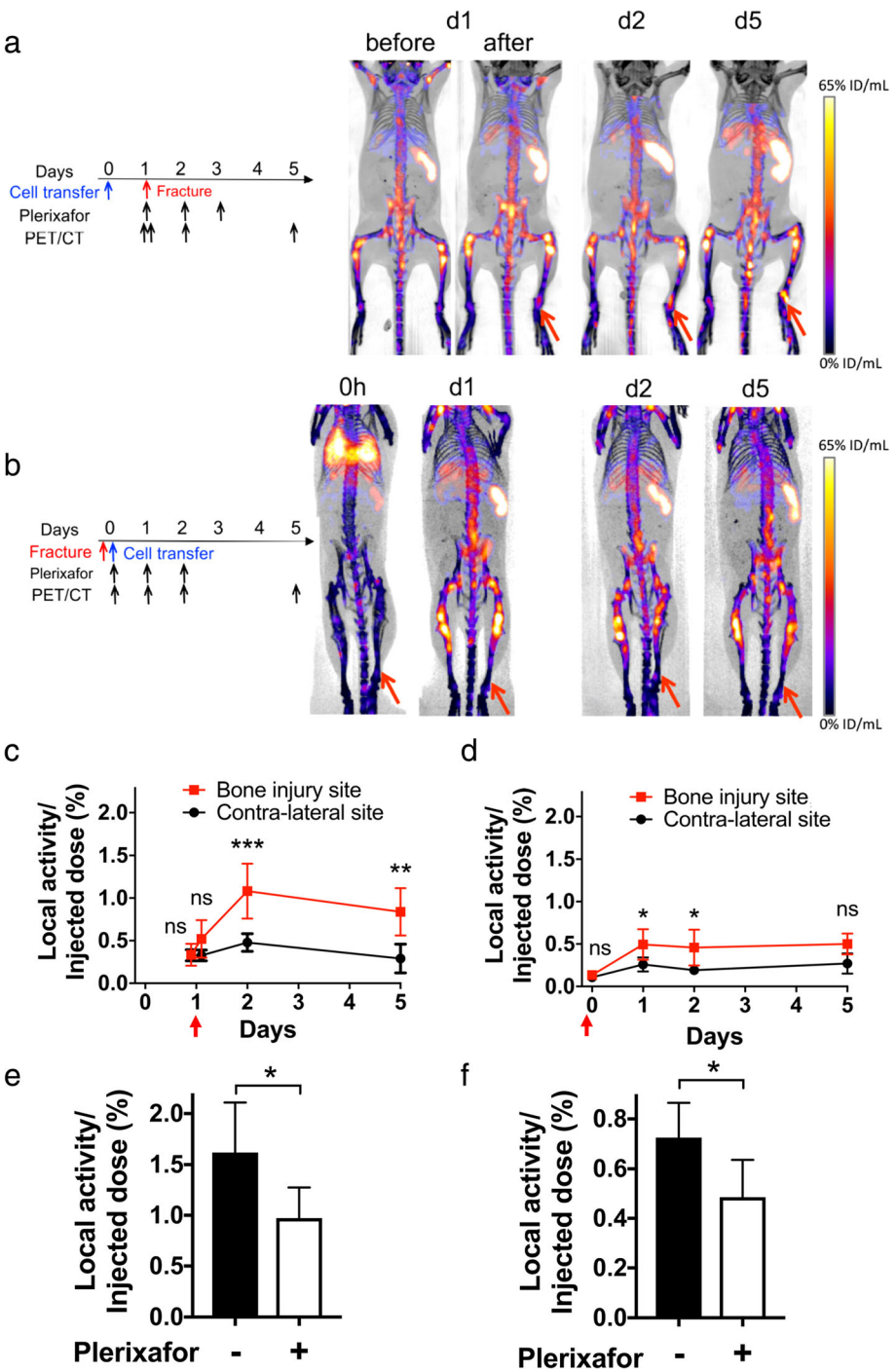

Fig. 3 Mobilization of BM cells using plerixafor reduces cell migration to the site of fracture. **a** The regimen of d1-fracture with a 3-day administration of plerixafor starting on day 1 and microPET/CT images are shown. ^{89}Zr-oxine-labeled BM cells trafficked to the fracture site and the accumulation was observed on day 2 through day 5 ($n = 4$). **b** The regimen of d0-fracture with a 3-day administration of plerixafor starting on day 0 and microPET/CT images are shown. The ^{89}Zr-oxine-labeled BM cells were transferred immediately after the fracture generation and administration of the first dose of plerixafor. Weak ^{89}Zr signal was observed at the injury site from day 1 through day 5 ($n = 4$). **c** Quantitation of the d1-fracture-plerixafor PET images indicate that the percentage of ^{89}Zr-labeled BM cells accumulated at the fracture was significantly higher than in the contralateral non-fractured tibia ($n = 4$). **d** Quantitation of the d0-fracture-plerixafor PET images show a slightly higher ^{89}Zr-labeled BM cells accumulation at the fracture compared to the contralateral tibia ($n = 4$). (*ns* not significant, *$p < 0.05$, **$p < 0.01$, ***$p < 0.001$, two-way repeated measure ANOVA with Sidak's test. The arrows indicate the timing of bone injury generation). **e** The peak accumulation on day 2 was reduced by plerixafor compared to non-mobilized mice in the d1-fracture-plerixafor scheme ($n = 6$). **f** Plerixafor significantly reduce the peak accumulation, on day 1 and 2, compared to the non-mobilized mice in the d0-fracture-plerixafor scheme ($n = 6$). (*$p < 0.05$ with Mann-Whitney test)

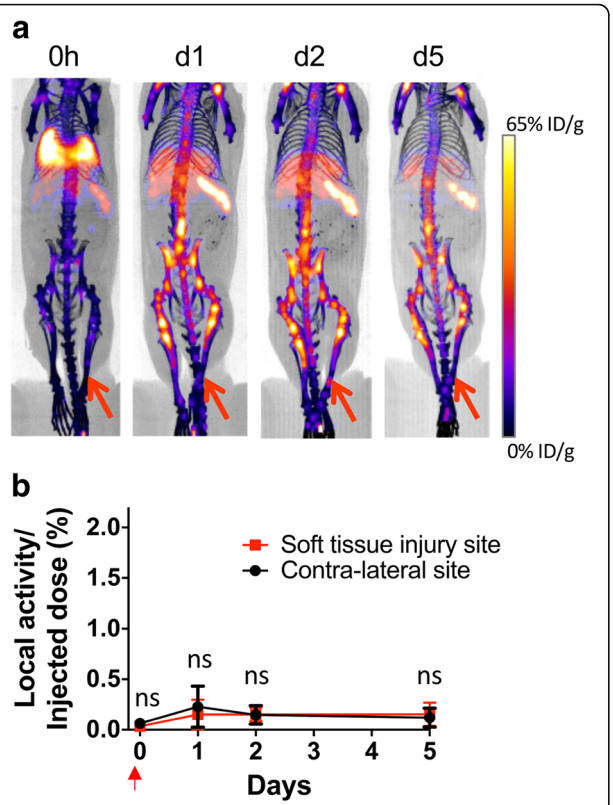

Fig. 4 Soft-tissue injury does not attract the BM cells. **a** A soft-tissue injury in the distal lower leg overlying the distal tibia was created and ^{89}Zr-labeled BM cells (2×10^7 cells at 9.65–21.3 kBq/10^6 cells) were transferred intravenously. MicroPET/CT images were acquired on days 0, 1, 2, and 5 ($n = 4$). **b** Soft-tissue incision without bone fracture did not recruit BM cells to the injury site. The arrow indicates the timing of soft-tissue injury generation

non-fractured tibias (Fig. 5c, d). In the analysis of non-hematopoietic cells including MSCs, d1-fracture site showed slightly higher $CD29^+CD105^+$ cells within $CD45^-$ donor cells than the contralateral control (Fig. 5e), but this was not statistically significant. As fracture is known to attract various inflammatory cells during the acute phase, we evaluated for monocytic and granulocytic myeloid cells in the injury region. Interestingly, we found that $CD11b^+Ly6C^{intermediate}Ly6G^+$ granulocytic myeloid cells rather than $CD11b^+Ly6C^+Ly6G^-$ monocytic myeloid cells migrated into the fracture (Fig. 5f, $p < 0.05$ in d1-fratured tibia vs control tibia, and Fig. 5g).

BM cells accumulated at the bone injury engraft and participate in fracture healing

Finally, we asked if the BM cells migrated to fracture were involved in fracture healing. To this end, histological sections of fractured and non-fractured contralateral tibias were prepared from fractured mice transferred with ^{89}Zr-oxine-labeled GFP^+ BM cells. H&E staining indicated inflammatory cells and fibrous tissue surrounding the fracture, and GFP-IHC demonstrated accumulation of GFP^+ cells in the fracture callus at 1.5 weeks (Fig.6a, b). At 7 weeks, the hard callus was formed and GFP^+ cells were present (Fig. 6c, d). In the non-fractured contralateral side, we observed fat marrow with negligible GFP^+ cells at day (Fig. 6e, f). A non-fractured tibia of GFP-transgenic and wild-type mouse that did not receive BM cell transplant is shown as controls (Fig. 6g, h, respectively). These histological observations support the concept that BM cells recruited to sites of injury are incorporated into the repair process.

Discussion

The ability to radiolabel hematopoietic cells without interfering with their viability, chemotaxis, or ability to differentiate is a powerful method to understand the migration of such cells in vivo under a variety of conditions [16, 17]. Because PET cameras are more efficient than gamma cameras, it is possible to reduce the radioactivity needed to visualize hematopoietic cells in the body thereby causing less damage to the cells. In this study, ^{89}Zr-oxine BM cell labeling was used to examine the migration of BM cells to an acute tibial injury. Based on the previous extensive ^{89}Zr-oxine radiotoxicity evaluations on the BM cells [17], ^{89}Zr-oxine labeling doses were carefully controlled to be within the optimized range to avoid altering viability, proliferation, and more importantly, differentiation function of the cells. ^{89}Zr was stably retained with the BM cells [17]. Two scenarios were employed: d1-fracture in which BM cell transfer preceded the fracture by 1 day and d0-fracture in which the fracture preceded the transfer of BM cells. With the d1-fracture regimen, we examined the effect of the fracture on the bone marrow cells already distributed to the organs and reached the steady state. The d0-fracture regimen, on the other hand, addressed the effect of fracture on the circulating bone marrow cells. In both conditions, ^{89}Zr-oxine-labeled cells accumulated at the site of tibial injury, peaking by approximately 24 h at 0.7–1.7% of the administered cells. While representing a minority of injected cells, this small number of cells is readily detected on PET imaging (Figs. 1b, c and 3a, b) with extremely high signal-to-background SUV ratios (Additional file 1: Figures S1a, b and S2a, b). As about 17% of the transferred cells migrated to the bone marrow (Additional file 1: Figures S1c, d and S2c, d), the percentage of cells accumulated at the injury was equivalent to as high as 4–10% of the cells in the bone marrow. After reaching the peak accumulation, the BM cells at the fracture gradually decreased. This is likely because the death of some cells that failed to engraft, even if they migrated to the injury sites. The distribution of the cells to the BM, spleen, and liver, observed within 24 h in

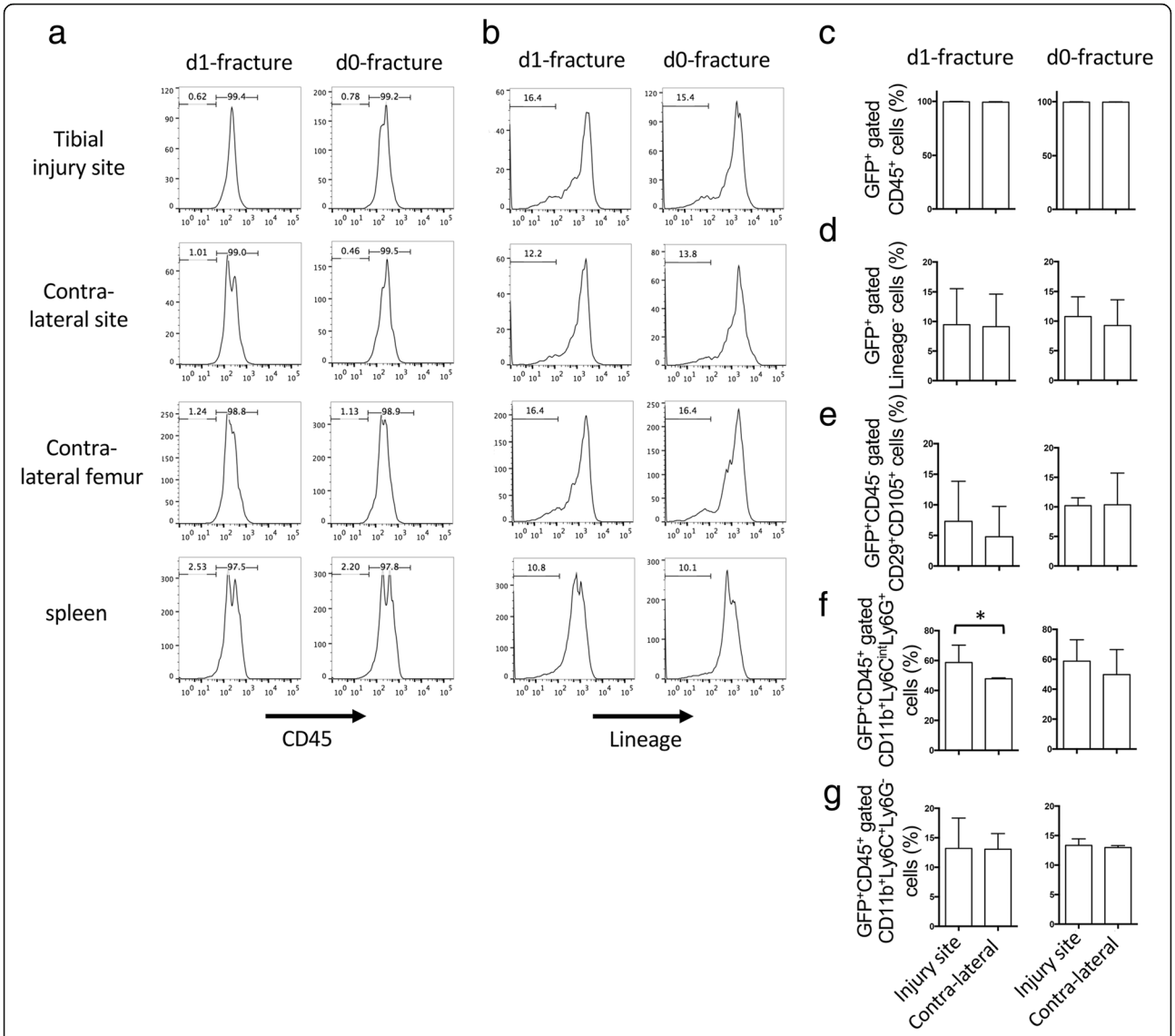

Fig. 5 Flow cytometry analysis demonstrates that the donor BM cells homing to the fracture site are mostly hematopoietic cells stem/progenitor cells and inflammatory cells. **a** BM cells from GFP transgenic mice were used as donor cells in d1- and d0-fracture models. One day later, cells were harvested from the fractured section of the tibia, corresponding contralateral tibia section, BM from non-fracture side femur, and spleen ($n = 4$). Flow cytometry analysis indicated that almost all the GFP^+ cells found in these tissues expressed CD45 (representative data). **b** The fraction of Lin^- cells in GFP^+ donor cells is indicated (representative data). **c**–**g** Comparison of cell fractions found in the sections of fractured vs non-fractured tibia is shown. $CD45^+$ cells (**c**) and Lin^- cells (**d**) within the donor cells, $CD29^+CD105^+$ cells within non-hematopoietic donor cells (**e**), $Ly6C^{intermediate\ (int)}$ $Ly6G^+$ cells (**f**), and $Ly6C^+Ly6G^-$ cells (**g**) within $CD11b^+$ donor cells were analyzed. $Ly6C^{int}Ly6G^+$ cells migrated to the fracture significantly higher than the non-fractured tibia ($n = 4$ in each group, $^*p < 0.05$ with Mann-Whitney test)

both fracture models, was almost identical to that in non-fractured control mice.

It has been shown that the BM stromal cells and bone periosteal cells release SDF-1 from the periosteum in response to bone injury [9, 21–23]. SDF-1, along with other key cytokines, play an important role in recruiting various hematopoietic and mesenchymal stem/progenitor cell types to the injury site in order to facilitate tissue repair and regeneration [24–30]. SDF-1 expression increases shortly after injury [9, 29, 31, 32], leading to the recruitment of cells expressing CXCR4. Not surprisingly, in both the d1- and d0-fracture groups, we observed the rapid migration of BM cells to the tibial injury within 24 h (Fig. 1b, c) and the radioactivity remained relatively stable thereafter for up to 5 days of observation. The distal tibia was chosen as the site for injury because it is not associated with hematopoietic marrow, making it less likely a homing region for transplanted BM cells. This BM cell accumulation shown at the bone injury site was not observed in similar contralateral non-injured

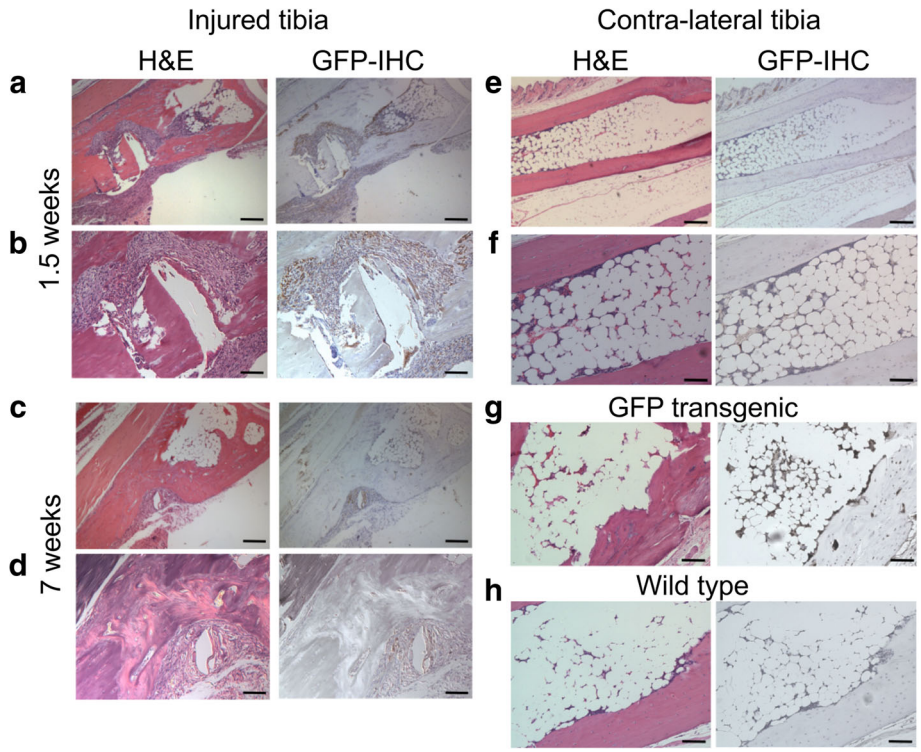

Fig. 6 GFP$^+$ donor cells are detected in the bone fracture. **a**, **b** BM cells from GFP transgenic mice were transferred to wild-type mice immediately after tibial fracture and 1.5 weeks later, the fractured tibia section and corresponding contralateral tibia section were harvested. Tissues slices were stained with H&E and with GFP-IHC. Microscopic images of fractured tibia indicated that the fractured bone was surrounded by inflammatory tissue (**a**, **b**, left, H&E) and GFP$^+$ donor cells were engrafted around the fracture (**a**, **b**, right, GFP-IHC). **c**, **d** Tissue sections created at 7 weeks following the bone marrow cell transfer indicated callus formation with GFP$^+$ cells in the surrounding soft-tissue (left: H&E, right: GFP-IHC). **e**, **f** Contralateral non-fractured tibia at 1.5 weeks after the cell transfer is shown. **g**, **h** Tibia from a GFP$^+$ (**g**) and a wild-type (**h**) mice are shown as controls. Scale bar indicates 200 μm in (**a**, **c**) and (**e**), and 100 μm in (**b**, **d**, **f**, **g**) and (**h**)

areas nor in mice that received only superficial injury to the soft-tissue overlying the tibia (Fig.4), supporting the model of SDF-1 production by periosteum after the bone injury [21, 22]. This suggests that bone injury induces a unique cell signaling cascade that recruits bone marrow cells to the injury to promote healing. In this regard, the amount of the bone marrow cells recruited to the injury may be affected by the size and depth of the bone injury.

Multiple groups have reported stem and progenitor cell recruitment, engraftment, and differentiation into bone-forming cells following CXCR4 blockade and subsequent mobilization of CXCR4$^+$ cells from the BM niche into the circulation [11, 13, 33, 34]. We have previously demonstrated mobilization of ^{89}Zr-oxine-labeled BM cells into peripheral blood by a CXCR4 blocker, plerixafor, using both PET imaging and flow cytometry analysis [17]. In the case of acute bone injury, it is thought that stem cells mobilized from the BM niche by plerixafor migrate to the fracture site in greater numbers. In both d1- and d0-fracture models, we observed an overall *inhibition* in BM cell uptake at the bone injury site, by as much as 33–40% by day 2, after plerixafor (Fig. 3e, f). It is critical that CXCR4$^+$ cells migrate and engraft using the SDF-1 chemokine gradient secreted by stromal cells in the injured bone periosteum. Thus, it appears that while CXCR4 blockade with plerixafor released more BM cells into the circulation, it also inhibited BM cell chemotaxis to the fracture site, leading to a net decrease in cell accumulation. These findings support previous reports suggesting that plerixafor acts to block CXCR4$^+$ cell migration toward SDF-1 producing stromal cells during the acute phase of fracture healing and, therefore, may be detrimental [35].

Because labeled donor cells constituted a small fraction of the progenitor cell population in comparison to the native host cells, it is very likely that the donor cells in the d0-fracture mice were just beginning to make their way into the arterial circulation to home to their eventual tissue destinations, when endogenous CXCR4$^+$ cells were mobilized to home to the fracture site. Thus, this model likely underestimates the actual accumulation of BM cells at the fracture site and

would explain why we observed a reduced donor cell uptake in the d0-fracture mice compared to the d1-fracture mice.

MSCs, primarily osteoblast progenitor cells, and as well as hematopoietic cells have been shown to migrate to the site of fracture during bone repair [19–21, 36]. In order to determine which BM cell types homed to the fracture, we performed flow cytometry 2 days after the cell transfer, corresponding to the peak accumulation of cells. Cells were isolated from a small section of tibia at both the fracture site and the contralateral normal site, as well as the normal femur and the spleen. GFP served as a marker for the donor cells. Across these tissue types, almost all of the donor cells were $CD45^+$ hematopoietic cells; however, $CD45^-CD29^+CD105^+$ cells that are likely to be MSCs or endothelial cells were also present (Fig. 5). We also observed preferential migration of granulocytic myeloid cells to the fracture in the d1-fracture model (Fig. 5f). In these flow cytometry analyses, it is possible that the specificity of cell types migrating to the fracture was significantly underestimated due to the inclusion of surrounding non-fractured tibia, causing a large "dilution" effect. We only analyzed the presence of donor cells early after their transfer, and thus, there may be some donor cell types that migrate to the fracture later and therefore, were not captured by our analysis. In addition, flow cytometry analysis after 6–7 weeks of healing, when the cells would have been fully differentiated, may reveal greater differences in marker expression on donor cells in the fracture site vs. contralateral site.

Finally, we did confirm that donor cells successfully engrafted in the healing fractured-tibia using immunohistochemistry (Fig. 6). Ten days after the fracture, the donor cells contributed to the inflammatory tissue formation which eventually enters the soft callus phase. At 7 weeks, the GFP^+ cells were still detectable around the callus at the fracture site.

Conclusions

BM cell ^{89}Zr-oxine-labeling with microPET/CT imaging revealed that acute fracture results in the redistribution of BM cells to the fracture within 24 h. Our data strongly suggests that BM mobilization occurs rapidly after fracture and that hematopoietic cells are the first cells to arrive at the bone fracture. Furthermore, our study indicated that CXCR4 blockade negatively affected BM cell migration toward the fracture site at least in the early phase of fracture healing. PET imaging enabled visualization and quantitation of in vivo BM cell trafficking and homing to various tissues, including the bone fracture site, making it a useful tool in understanding the bone marrow response to acute bone fracture.

Additional file

Additional file 1: Figure S1. BM cells accumulated at the bone injury show high ^{89}Zr signals by microPET/CT imaging. Figure S2. Mobilization of BM cells using plerixafor reduces ^{89}Zr signals at the site of bone injury. (ZIP 1575 kb)

Abbreviations

^{89}Zr: Zirconium-89; ACK: Ammonium-chloride-potassium; ANOVA: Analysis of variance; BM: Bone marrow; CT: Computed tomography; EPCs: Endothelial progenitor cells; GFP: Green fluorescence protein; H&E: Hematoxylin and eosin; HSCs: Hematopoietic stem cells; IHC: Immunohistochemistry; IL: Interleukin; MSCs: Mesenchymal stem cells; PBS: Phosphate-buffered saline; PET: Positron emission tomography; SDF-1: Stromal cell-derived factor-1; SUV: Standardized uptake value; TNF-α: Tumor necrosis factor-α

Acknowledgements

Not applicable.

Funding

This research was supported by the Intramural Research Program of the National Institutes of Health, National Cancer Institute, Center for Cancer Research. K.O.A. was an awardee of the National Institutes of Health Undergraduate Scholarship Program.

Availability of data and materials

The datasets generated during the current study are included in this published article.

Authors' contributions

KOA designed and performed research, collected, analyzed and interpreted data, performed statistical analysis, and wrote the manuscript. MF performed experiments and collected and analyzed data. PTT and SSA analyzed data and wrote the manuscript. PLC interpreted data and wrote the manuscript, and NS designed and performed research, collected, analyzed and interpreted data, performed statistical analysis, and wrote the manuscript. KOA and NS are responsible for the integrity of the data analysis. All authors read and approved the final manuscript.

Author's information

Regarding S.S.A., this project has been funded in whole or in part with federal funds from the National Cancer Institute, National Institutes of Health, under Contract No. HHSN261200800001E. The content of this publication does not necessarily reflect the views or policies of the Department of Health and Human Services, nor does mention of trade names, commercial products, or organizations imply endorsement by the U.S. Government.

Ethics approval

All animal experiments were performed in accordance with a protocol approved by the institutional Animal Care and Use Committee.

Consent for publication

Not applicable.

Competing interests

The authors N.S. and P.L.C. have filed U.S. and International Patent Applications for generation and application of the ^{89}Zr-oxine complex for PET imaging.

Publisher's Note

Author details

[1]Molecular Imaging Program, Center for Cancer Research, National Cancer Institute, National Institutes of Health, NIH, Building 10, Room B3B406, Bethesda, MD 20892-1002, USA. [2]Clinical Monitoring Research Program Directorate, Frederick National Laboratory for Cancer Research sponsored by the National Cancer Institute, Frederick, MD 21702, USA.

Received: 1 October 2018 Accepted: 26 November 2018
Published online: 13 December 2018

References

1. Gerstenfeld LC, Cho TJ, Kon T, Aizawa T, Tsay A, Fitch J, et al. Impaired fracture healing in the absence of TNF-alpha signaling: the role of TNF-alpha in endochondral cartilage resorption. J Bone Miner Res. 2003;18(9):1584–92.
2. Einhorn TA, Majeska RJ, Rush EB, Levine PM, Horowitz MC. The expression of cytokine activity by fracture callus. J Bone Miner Res. 1995;10(8):1272–81.
3. Einhorn TA. The cell and molecular biology of fracture healing. Clin Orthop Relat Res. 1998;(355 Suppl):S7–21.
4. Loi F, Cordova LA, Pajarinen J, Lin TH, Yao Z, Goodman SB. Inflammation, fracture and bone repair. Bone. 2016;86:119–30.
5. Yellowley C. CXCL12/CXCR4 signaling and other recruitment and homing pathways in fracture repair. Bonekey Rep. 2013;2:300.
6. Ferretti C, Borsari V, Falconi M, Gigante A, Lazzarini R, Fini M, et al. Human periosteum-derived stem cells for tissue engineering applications: the role of VEGF. Stem Cell Rev. 2012;8(3):882–90.
7. Choi YS, Noh SE, Lim SM, Lee CW, Kim CS, Im MW, et al. Multipotency and growth characteristic of periosteum-derived progenitor cells for chondrogenic, osteogenic, and adipogenic differentiation. Biotechnol Lett. 2008;30(4):593–601.
8. De Bari C, Dell'Accio F, Vanlauwe J, Eyckmans J, Khan IM, Archer CW, et al. Mesenchymal multipotency of adult human periosteal cells demonstrated by single-cell lineage analysis. Arthritis Rheum. 2006;54(4):1209–21.
9. Ceradini DJ, Kulkarni AR, Callaghan MJ, Tepper OM, Bastidas N, Kleinman ME, et al. Progenitor cell trafficking is regulated by hypoxic gradients through HIF-1 induction of SDF-1. Nat Med. 2004;10(8):858–64.
10. Sordi V, Malosio ML, Marchesi F, Mercalli A, Melzi R, Giordano T, et al. Bone marrow mesenchymal stem cells express a restricted set of functionally active chemokine receptors capable of promoting migration to pancreatic islets. Blood. 2005;106(2):419–27.
11. Wang XX, Allen RJ Jr, Tutela JP, Sailon A, Allori AC, Davidson EH, et al. Progenitor cell mobilization enhances bone healing by means of improved neovascularization and osteogenesis. Plast Reconstr Surg. 2011;128(2):395–405.
12. Kumar S, Ponnazhagan S. Mobilization of bone marrow mesenchymal stem cells in vivo augments bone healing in a mouse model of segmental bone defect. Bone. 2012;50(4):1012–8.
13. Toupadakis CA, Granick JL, Sagy M, Wong A, Ghassemi E, Chung DJ, et al. Mobilization of endogenous stem cell populations enhances fracture healing in a murine femoral fracture model. Cytotherapy. 2013;15(9):1136–47.
14. Toupadakis CA, Wong A, Genetos DC, Chung DJ, Murugesh D, Anderson MJ, et al. Long-term administration of AMD3100, an antagonist of SDF-1/CXCR4 signaling, alters fracture repair. J Orthop Res. 2012;30(11):1853–9.
15. Kitaori T, Ito H, Schwarz EM, Tsutsumi R, Yoshitomi H, Oishi S, et al. Stromal cell-derived factor 1/CXCR4 signaling is critical for the recruitment of mesenchymal stem cells to the fracture site during skeletal repair in a mouse model. Arthritis Rheum. 2009;60(3):813–23.
16. Sato N, Wu H, Asiedu KO, Szajek LP, Griffiths GL, Choyke PL. (89)Zr-Oxine complex PET cell imaging in monitoring cell-based therapies. Radiology. 2015;275(2):490–500.
17. Asiedu KO, Koyasu S, Szajek LP, Choyke PL, Sato N. Bone marrow cell trafficking analyzed by (89)Zr-oxine positron emission tomography in a murine transplantation model. Clin Cancer Res. 2017;23(11):2759–68.
18. Kumagai K, Vasanji A, Drazba JA, Butler RS, Muschler GF. Circulating cells with osteogenic potential are physiologically mobilized into the fracture healing site in the parabiotic mice model. J Orthop Res. 2008;26(2):165–75.
19. Mehrotra M, Williams CR, Ogawa M, LaRue AC. Hematopoietic stem cells give rise to osteo-chondrogenic cells. Blood Cells Mol Dis. 2013;50(1):41–9.
20. Kuroda R, Matsumoto T, Kawakami Y, Fukui T, Mifune Y, Kurosaka M. Clinical impact of circulating CD34-positive cells on bone regeneration and healing. Tissue Eng B Rev. 2014;20(3):190–9.
21. Otsuru S, Tamai K, Yamazaki T, Yoshikawa H, Kaneda Y. Circulating bone marrow-derived osteoblast progenitor cells are recruited to the bone-forming site by the CXCR4/stromal cell-derived factor-1 pathway. Stem cells (Dayton, Ohio). 2008;26(1):223–34.
22. Matsumoto T, Mifune Y, Kawamoto A, Kuroda R, Shoji T, Iwasaki H, et al. Fracture induced mobilization and incorporation of bone marrow-derived endothelial progenitor cells for bone healing. J Cell Physiol. 2008;215(1):234–42.
23. Lee DY, Cho TJ, Kim JA, Lee HR, Yoo WJ, Chung CY, et al. Mobilization of endothelial progenitor cells in fracture healing and distraction osteogenesis. Bone. 2008;42(5):932–41.
24. Seebach C, Henrich D, Tewksbury R, Wilhelm K, Marzi I. Number and proliferative capacity of human mesenchymal stem cells are modulated positively in multiple trauma patients and negatively in atrophic nonunions. Calcif Tissue Int. 2007;80(4):294–300.
25. Zvaifler NJ, Marinova-Mutafchieva L, Adams G, Edwards CJ, Moss J, Burger JA, et al. Mesenchymal precursor cells in the blood of normal individuals. Arthritis Res. 2000;2(6):477–88.
26. Mansilla E, Marin GH, Drago H, Sturla F, Salas E, Gardiner C, et al. Bloodstream cells phenotypically identical to human mesenchymal bone marrow stem cells circulate in large amounts under the influence of acute large skin damage: new evidence for their use in regenerative medicine. Transplant Proc. 2006;38(3):967–9.
27. Undale A, Srinivasan B, Drake M, McCready L, Atkinson E, Peterson J, et al. Circulating osteogenic cells: characterization and relationship to rates of bone loss in postmenopausal women. Bone. 2010;47(1):83–92.
28. Alm JJ, Koivu HM, Heino TJ, Hentunen TA, Laitinen S, Aro HT. Circulating plastic adherent mesenchymal stem cells in aged hip fracture patients. J Orthop Res. 2010;28(12):1634–42.
29. Ma J, Ge J, Zhang S, Sun A, Shen J, Chen L, et al. Time course of myocardial stromal cell-derived factor 1 expression and beneficial effects of intravenously administered bone marrow stem cells in rats with experimental myocardial infarction. Basic Res Cardiol. 2005;100(3):217–23.
30. Khosla S, Eghbali-Fatourechi GZ. Circulating cells with osteogenic potential. Ann N Y Acad Sci. 2006;1068:489–97.
31. Togel F, Isaac J, Hu Z, Weiss K, Westenfelder C. Renal SDF-1 signals mobilization and homing of CXCR4-positive cells to the kidney after ischemic injury. Kidney Int. 2005;67(5):1772–84.
32. De Falco E, Porcelli D, Torella AR, Straino S, Iachininoto MG, Orlandi A, et al. SDF-1 involvement in endothelial phenotype and ischemia-induced recruitment of bone marrow progenitor cells. Blood. 2004;104(12):3472–82.
33. Liu X, Zhou C, Li Y, Ji Y, Xu G, Wang X, et al. SDF-1 promotes endochondral bone repair during fracture healing at the traumatic brain injury condition. PLoS One. 2013;8(1):e54077.
34. Dimitriou R, Tsiridis E, Giannoudis PV. Current concepts of molecular aspects of bone healing. Injury. 2005;36(12):1392–404.
35. Sanghani-Kerai A, McCreary D, Lancashire H, Osagie L, Coathup M, Blunn G. Stem cell interventions for bone healing: fractures and osteoporosis. Curr Stem Cell Res Ther. 2018;13(5):369–77.
36. Kovach TK, Dighe AS, Lobo PI, Cui Q. Interactions between MSCs and immune cells: implications for bone healing. J Immunol Res. 2015;2015:752510.